nature chemical biology

ARTICLE

PUBLISHED ONLINE: 30 MARCH 2015 | DOI: 10.1038/NCHEMBIO.1786

A pentose bisphosphate pathway for nucleoside degradation in Archaea

Riku Aono[1,2], Takaaki Sato[1,3], Tadayuki Imanaka[3,4] & Haruyuki Atomi[1,3]*

Owing to the absence of the pentose phosphate pathway, the degradation pathway for the ribose moieties of nucleosides is unknown in Archaea. Here, in the archaeon *Thermococcus kodakarensis*, we identified a metabolic network that links the pentose moieties of nucleosides or nucleotides to central carbon metabolism. The network consists of three nucleoside phosphorylases, an ADP-dependent ribose-1-phosphate kinase and two enzymes of a previously identified NMP degradation pathway, ribose-1,5-bisphosphate isomerase and type III ribulose-1,5-bisphosphate carboxylase/oxygenase. Ribose 1,5-bisphosphate and ribulose 1,5-bisphosphate are intermediates of this pathway, which is thus designated the pentose bisphosphate pathway.

The pentose phosphate pathway[1,2] is considered a ubiquitous pathway in bacteria and eukaryotes. It provides the reducing equivalents (NADPH) necessary for various biosynthetic pathways and generates erythrose 4-phosphate, a precursor for aromatic amino acid and folate biosynthesis. The pathway is also responsible for the interconversion of pentoses necessary for nucleic acid biosynthesis and the trioses and hexoses found in glycolysis and gluconeogenesis (**Fig. 1a**). It is known that many archaea do not harbor a complete pentose phosphate pathway[3]. In terms of pentose synthesis from trioses and hexoses, the ribulose monophosphate pathway substitutes the pentose phosphate pathway in Archaea[4]. However, a route through which the pentose moieties from nucleosides are directed to the trioses and hexoses in glycolysis and gluconeogenesis has not been demonstrated.

Many archaea harbor a type III ribulose-1,5-bisphosphate carboxylase/oxygenase (Rubisco) that exhibits carboxylase activity but does not participate in the Calvin-Benson-Bassham cycle[5–9]. Biochemical analyses suggest that the type III Rubisco from the hyperthermophilic archaeon *T. kodakarensis* participates in a metabolic pathway involved in nucleoside 5′-monophosphate (NMP) degradation, together with two enzymes specific to Archaea, AMP phosphorylase (AMPpase) and ribose-1,5-bisphosphate isomerase (R15P isomerase)[10–13]. AMPpase catalyzes the phosphorolysis of AMP, CMP and UMP, releasing the corresponding bases and generating ribose 1,5-bisphosphate (R15P). R15P is subsequently isomerized to ribulose 1,5-bisphosphate (RuBP) by R15P isomerase. RuBP, CO_2 and H_2O are then converted to two molecules of 3-phosphoglycerate (3-PGA) by type III Rubisco (**Fig. 1b**). The conversion of AMP, CMP and UMP to 3-PGA is also observed in *T. kodakarensis* cell extracts. The data suggest that in *T. kodakarensis*, AMP, CMP and UMP are degraded via this NMP degradation pathway involving AMPpase, R15P isomerase and Rubisco. The first two reactions are reversible, but the irreversible Rubisco reaction directs the metabolic flow of the pathway toward NMP degradation. The second enzyme, R15P isomerase, is activated by AMP and exhibits only trace levels of activity in its absence[13]. This is presumed to be a feed-forward control mechanism to enhance NMP degradation when AMP is abundant and to block NMP degradation when AMP levels are low.

In addition, R15P isomerase and Rubisco, but not AMPpase, are induced upon addition of nucleosides to the medium[13]. This suggests that these two enzymes are also involved in nucleoside metabolism. In this study, we examined the involvement of the NMP degradation pathway in nucleoside metabolism and found that the pathway in *T. kodakarensis* is a part of a larger metabolic network that links the ribose moieties of nucleosides to central carbon metabolism (**Fig. 1b**).

RESULTS

Candidates for nucleoside kinases in *T. kodakarensis*

To gain insight into the participation of the NMP degradation pathway in nucleoside metabolism, we examined whether nucleoside kinases were present in *T. kodakarensis*. Nucleoside kinases would convert nucleosides to NMPs, which are the substrates for the NMP degradation pathway. We identified two candidates on the *T. kodakarensis* genome, TK1843 and TK2029, that were 18–28% identical to three previously identified archaeal nucleoside kinases, MJ0406 from *Methanocaldococcus jannaschii*[14], APE0012 from *Aeropyrum pernix*[14] and Ta0880 from *Thermoplasma acidophilum*[15]. The amino acid sequences of these proteins indicated that they were members of the ribokinase family[16]. We expressed the TK1843 and TK2029 genes in *Escherichia coli* and purified the recombinant proteins to apparent homogeneity (**Supplementary Results**, **Supplementary Fig. 1**). We examined ATP-dependent kinase activity by measuring the generation of ADP in a reaction mixture that contained ATP, substrate candidates and purified enzyme and that was coupled with pyruvate kinase/lactate dehydrogenase (**Table 1**). We applied high concentrations of enzyme (1.6 μM) so that low levels of activity toward any substrate would not be overlooked. We subtracted the ADP levels found in reactions carried out without enzyme in each assay to exclude trace levels of contaminant ADP present in commercially available ATP and any ADP generated by thermal degradation of ATP. In the case of the TK1843 protein, we observed ADP generation in the presence of cytidine and, to a lower extent, deoxycytidine and uridine. Using HPLC, we confirmed that the product of the reaction with cytidine was CMP (**Supplementary Fig. 2**). This was also supported by the generation of R15P when the reaction was coupled with AMPpase activity (**Supplementary Table 1**).

For the TK2029 protein, we were not able to observe high levels of ADP generation with any of the substrates examined, although trace levels of ADP were detected with deoxyribose 1-phosphate (dR1P). Notably, we observed that when ribose 1-phosphate (R1P)

[1]Department of Synthetic Chemistry and Biological Chemistry, Graduate School of Engineering, Kyoto University, Kyoto, Japan. [2]Japan Society for the Promotion of Science, Tokyo, Japan. [3]Japan Science and Technology Agency (JST), Core Research for Evolutional Science and Technology, Tokyo, Japan. [4]Department of Biotechnology, College of Life Sciences, Ritsumeikan University, Kyoto, Japan *e-mail: atomi@sbchem.kyoto-u.ac.jp

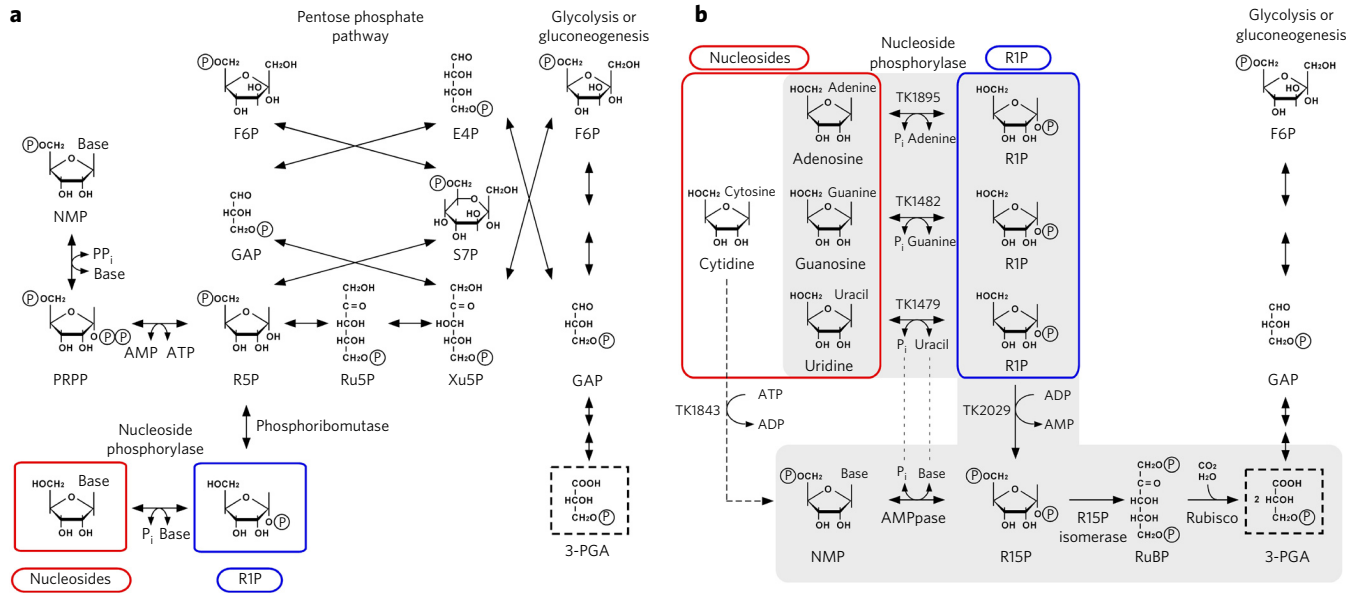

Figure 1 | Nucleoside metabolism in Archaea, Bacteria and Eukarya. (**a**) Classical nucleoside metabolism in Bacteria and Eukarya. The nonoxidative pentose phosphate pathway and a portion of glycolysis and gluconeogenesis pathway are indicated. (**b**) The metabolic network in *T. kodakarensis* identified in this study is shaded in gray. Genes encoding enzymes identified in this study are indicated with the corresponding gene numbers. Solid arrows indicate reaction steps that have been genetically confirmed with cell extracts. The cytidine kinase reaction has not been confirmed and is indicated with a dotted arrow. A portion of the glycolysis and gluconeogenesis pathway is indicated. GAP, glyceraldehyde 3-phosphate; F6P, fructose 6-phosphate; PPi, pyrophosphate; PRPP, phosphoribosylpyrophosphate; Xu5P, xylulose 5-phosphate; S7P, sedoheptulose 7-phosphate; E4P, erythrose 4-phosphate.

was used as the substrate, ADP levels in the reaction mixture were lower with substrate than without. We thus examined whether TK2029 used ADP as the phosphate donor. Indeed, we observed high levels of AMP formation when the TK2029 protein was incubated with R1P or dR1P (**Table 1** and **Supplementary Fig. 3**). The reaction product with R1P was converted to 3-PGA by R15P isomerase and Rubisco, indicating that it was R15P (**Supplementary Table 2**). The results indicated that the TK2029 protein uses ADP as the phosphate donor. In a number of archaea, including *T. kodakarensis*, the glucokinase and phosphofructokinase in the modified Embden-Meyerhof pathway use ADP for sugar phosphorylation[17–23]. An ADP-dependent glucokinase is known to be present in mouse cells[24]. Furthermore, another enzyme from *E. coli*, an NAD(P)HX dehydratase, whose overall dehydration reaction includes an initial phosphorylation step, uses ADP as the phosphate donor[25]. These findings indicate that the use of ADP as a phosphate donor occurs in all three domains of life and may be more widespread than had been previously recognized.

ATP-dependent cytidine kinase

As we were able to identify substrates for the TK1843 and TK2029 proteins, we examined their enzymatic properties in detail. For the TK1843 protein that displayed kinase activity toward cytidine, deoxycytidine and uridine, we detected relatively high levels of activity within a broad pH range of 5.0–9.0 (**Supplementary Fig. 4**) and maximum activity at 90 °C. Addition of 300 mM KCl led to a 3.6-fold increase in activity (**Supplementary Fig. 5**). The activation energy calculated from activity levels measured at temperatures ranging from 60 °C to 90 °C indicated a value of 83.0 kJ mol^{-1} (**Supplementary Fig. 6**). When we examined the specificity for the phosphate donor at 5 mM, we found that ATP was the most preferred donor (**Supplementary Fig. 7**). We also observed high levels of activity with GTP, which was nearly 70% of the activity observed with ATP. The levels of activity with CTP and UTP were both approximately 30% of that with ATP. Mg^{2+} was the most preferred divalent cation, followed by Mn^{2+} (68% of the activity levels observed with Mg^{2+}) and Co^{2+} (26%; **Supplementary Fig. 8**). Activity levels with Ca^{2+}, Ni^{2+}, Zn^{2+} and Cu^{2+} were all less than 20%. We observed precipitation in the reaction mixture in the presence of Mn^{2+}, Co^{2+} and Ni^{2+}. We carried out kinetic analyses with the phosphate acceptors cytidine and deoxycytidine using ATP as the phosphate donor (**Supplementary Fig. 9a**). We observed substrate inhibition in the case of cytidine, but higher activity was observed with cytidine than with deoxycytidine at concentrations up to 10 mM. We calculated the kinetic parameters of the reactions using the Michaelis-Menten equation for deoxycytidine and using the equation $v = V_{max}[S]/(K_s+[S]+[S]^2/K_i)$ for cytidine, where v is initial velocity, V_{max} is maximum velocity, [S] is cytidine concentration, K_s is the dissociation constant of the substrate, and K_i is the dissociation constant of the inhibitory substrate (**Table 2**). We also examined activity with varying concentrations of ATP and GTP using cytidine as the phosphate acceptor. Activity levels with ATP and GTP were similar up to concentrations of 5 mM, but we observed a strong substrate inhibition in the case of GTP (**Supplementary Fig. 9b**). The equation $v = V_{max}[S]/(K_s+[S]+[S]^2/K_i)$ did not fit well with the data. Although we were unable to propose an optimal model or equation, we observed that activity with ATP was higher than that with GTP at all concentrations. In summary, the results suggested that the TK1843 protein prefers ATP as the phosphate donor, cytidine as the phosphate acceptor and Mg^{2+} as the divalent cation.

ADP-dependent R1P kinase

As for the TK2029 protein that exhibited ADP-dependent R1P or dR1P kinase activity, we observed relatively high activity in the range of pH 5.0 to 8.0 (**Supplementary Fig. 10**) and maximum activity at 85 °C. Addition of 10 mM KCl resulted in a 2.7-fold increase in activity (**Supplementary Fig. 11**). The calculated activation energy of the reaction was 40.0 kJ mol^{-1} (**Supplementary Fig. 12**). Among the four NDPs, ADP was the most preferred, followed by GDP (56%) and UDP (9%; **Supplementary Fig. 13**). We did not observe activity with CDP and pyrophosphate. Mg^{2+} and Ca^{2+} (107% of the activity levels observed with Mg^{2+}) were the most preferred

Table 1 | Substrate specificities of the TK1843 protein and the TK2029 protein

		TK1843	TK2029	
Substrate		ADP generation from ATP (mM)	ADP generation from ATP (mM)	AMP generation from ADP (mM)
Nucleoside	Adenosine	0.01 ± 0.02	0.01 ± 0.01	0.14 ± 0.06
	Cytidine	4.83 ± 0.04	0.00 ± 0.00	0.00 ± 0.03
	Guanosine	−0.03 ± 0.03	−0.04 ± 0.02	0.12 ± 0.10
	Uridine	1.34 ± 0.12	0.01 ± 0.00	0.01 ± 0.01
	Inosine	0.01 ± 0.03	0.00 ± 0.01	0.15 ± 0.03
	Xanthosine	0.00 ± 0.01	−0.01 ± 0.00	0.14 ± 0.01
	Deoxyadenosine	0.00 ± 0.01	0.00 ± 0.01	0.17 ± 0.06
	Deoxycytidine	2.63 ± 0.14	0.00 ± 0.01	0.02 ± 0.02
	Deoxyguanosine	0.00 ± 0.02	−0.01 ± 0.00	0.14 ± 0.07
	Deoxyuridine	0.11 ± 0.01	0.01 ± 0.00	0.22 ± 0.10
	Deoxythymidine	0.01 ± 0.02	0.01 ± 0.01	0.03 ± 0.03
Sugar phosphate	R1P	0.00 ± 0.02	−0.16 ± 0.00	3.35 ± 0.20
	dR1P	−0.02 ± 0.01	0.12 ± 0.00	2.48 ± 0.07
	R5P	−0.01 ± 0.02	−0.02 ± 0.00	0.02 ± 0.03
	Glucose 1-phosphate	−0.03 ± 0.02	−0.02 ± 0.01	0.02 ± 0.03
	Glucose 6-phosphate	−0.03 ± 0.02	−0.02 ± 0.01	0.01 ± 0.02
	Fructose 6-phosphate	−0.02 ± 0.00	−0.01 ± 0.01	0.06 ± 0.01
Monosaccharide	Ribose	−0.02 ± 0.02	−0.01 ± 0.01	0.00 ± 0.03
	Fructose	−0.01 ± 0.02	−0.02 ± 0.01	0.00 ± 0.03
	Xylose	−0.01 ± 0.01	−0.02 ± 0.01	0.00 ± 0.01
	Erythrose	−0.02 ± 0.02	−0.03 ± 0.00	−0.01 ± 0.03
	Glucose	−0.01 ± 0.01	0.00 ± 0.01	0.01 ± 0.03
	Galactose	−0.01 ± 0.02	−0.02 ± 0.01	0.01 ± 0.03
	D-Arabinose	−0.01 ± 0.03	−0.01 ± 0.02	0.01 ± 0.03
	L-Arabinose	−0.02 ± 0.01	−0.01 ± 0.01	0.00 ± 0.03
	Lyxose	0.00 ± 0.02	0.00 ± 0.01	0.02 ± 0.03
	Ribulose	−0.01 ± 0.02	−0.01 ± 0.02	0.01 ± 0.02
	Xylulose	−0.01 ± 0.02	−0.01 ± 0.01	0.02 ± 0.01
	Erythrulose	−0.03 ± 0.01	−0.02 ± 0.01	−0.01 ± 0.04
	Deoxyribose	−0.02 ± 0.02	−0.01 ± 0.01	0.03 ± 0.04
	Gluconate	−0.02 ± 0.02	−0.02 ± 0.00	0.06 ± 0.03

Reaction conditions and detection methods are described in the Online Methods. The ADP and AMP concentrations were calculated by subtracting the values obtained in reactions without substrates from those with substrates. The data represent the average of three independent experiments and are shown with the s.d.

divalent cations, followed by Co^{2+} (59%; **Supplementary Fig. 14**). Activity levels with Mn^{2+}, Ni^{2+}, Zn^{2+} and Cu^{2+} were all less than 20%. We observed precipitation in the reaction mixture in the presence of Mn^{2+}, Ca^{2+} and Zn^{2+}. We performed kinetic examinations for the phosphate donors ADP and GDP with R1P as the phosphate acceptor in the presence of either 60 mM Mg^{2+} or Ca^{2+} (**Supplementary Fig. 15a**). When we compared the results for ADP and GDP with Mg^{2+}, ADP was clearly the preferred phosphate donor. We carried out the same analysis in the presence of Ca^{2+} instead of Mg^{2+} with varying concentrations of ADP. With Ca^{2+}, however, making accurate measurements became extremely difficult at ADP concentrations of 20 mM or higher owing to precipitation in the reaction mixture. The kinetic parameters of the reactions for ADP and GDP are shown in **Table 2**. We calculated the parameters with Ca^{2+} as the divalent cation using either (i) the complete data set (ADP concentrations 0–60 mM) or (ii) only the data where ADP concentrations were 15 mM or less, at which precipitation was not observed. Kinetic analyses of the phosphate acceptors R1P and dR1P clearly indicated that the enzyme preferred R1P (**Supplementary Fig. 15b**). In summary, the results suggested that the TK2029 protein is specific for ADP as the phosphate donor and R1P as the phosphate acceptor and can use either Mg^{2+} or Ca^{2+} as the divalent cation. When we compared the kinetic parameters of the reaction to previously characterized ADP-dependent kinases, the K_m value toward R1P (0.53 mM) was similar to that reported for the ADP-dependent glucokinase and ADP-dependent phosphofructokinase from *Pyrococcus furiosus* toward glucose (0.73 mM)[18] and fructose 6-phosphate (2.3 mM)[19], respectively. We also observed that the K_m value toward ADP (7.3 mM) was high compared to that of other ADP-dependent kinases from *P. furiosus*[18,19], *M. jannaschii*[20] and *Methanococcus maripaludis*[23] (0.032–1.2 mM). This may be somewhat due to the fact that our measurements were performed at 85 °C, whereas previously reported values were based on measurements that were performed at 30–50 °C (ref. 26). More notably, the relative concentration between ADP and the divalent cation has been reported to have a large impact on the catalytic properties of ADP-dependent glucokinases from *P. furiosus* and *Thermococcus litoralis* and the phosphofructokinase from *Pyrococcus horikoshii*[22], which may also be the case for the TK2029 protein reaction.

The ADP-dependent phosphorylation of R1P can be considered irreversible under physiological conditions, as in the case of ADP-dependent glucokinase and ADP-dependent phosphofructokinase[19,26]. When we examined the reverse reaction (ADP and R1P generation from AMP and R15P), at equilibrium we detected the generation of 0.06 ± 0.01 mM (mean ± s.d.) ADP from 5 mM AMP and 5 mM R15P. This corresponded to an equilibrium constant of $6.02 \pm 1.17 \times 10^3$ and a free energy difference of −25.9 ± 0.6 kJ mol^{-1} for the forward reaction, which was similar to the values obtained for ATP-dependent sugar kinases[27,28].

Our biochemical analyses indicated that the TK1843 protein is an ATP-dependent cytidine kinase. The TK2029 protein catalyzes a previously unidentified biological reaction, and we designated the enzyme as an ADP-dependent ribose-1-phosphate kinase (ADP-R1P kinase).

R15P generation from nucleosides in cell-free extracts

R1P, the substrate of ADP-R1P kinase, can be generated by nucleoside phosphorylases, enzymes commonly found in bacteria and eukaryotes. Nucleoside phosphorylases have also been identified and studied in archaeal species such as *P. furiosus*[29,30] and *Sulfolobus solfataricus*[31,32]. The archaeal proteins exhibit nucleoside phosphorylase activity, but their physiological roles are not known. Together with ADP-R1P kinase, the presence of nucleoside phosphorylases in *T. kodakarensis* may complement the absence of nucleoside kinase activity toward adenosine, guanosine and uridine. *T. kodakarensis* has three nucleoside phosphorylase homologs: TK1479 (annotated as uridine phosphorylase), TK1482 (purine nucleoside phosphorylase) and TK1895 (purine nucleoside phosphorylase)[33]. Although we originally anticipated

Table 2 | Kinetic parameters of the TK1843 and TK2029 proteins

Enzyme	Substrate	Metal (II)	K_m (mM)	K_i (mM)	V_{max} (μmol min^{-1} mg^{-1})	k_{cat} (s^{-1})	k_{cat}/K_m (s^{-1} mM^{-1})
TK1843	Cytidine	Mg^{2+}	1.71 ± 0.52	29.3 ± 13.4	552 ± 78	280 ± 40	164
	Deoxycytidine	Mg^{2+}	4.11 ± 0.52	-	446 ± 21	226 ± 11	55.0
	ATP	Mg^{2+}	5.72 ± 0.45	-	438 ± 12	222 ± 6	38.8
TK2029	R1P	Mg^{2+}	0.53 ± 0.13	-	912 ± 42	485 ± 22	915
	dR1P	Mg^{2+}	12 ± 9	-	137 ± 60	73 ± 32	6.28
	ADP	Mg^{2+}	7.3 ± 2.1	-	1150 ± 80	612 ± 43	83.6
	ADP	Ca^{2+} (1)	4.19 ± 1.01	-	1610 ± 80	856 ± 43	204
	ADP	Ca^{2+} (2)	8.37 ± 0.22	-	2180 ± 20	1160 ± 80	139
	GDP	Mg^{2+}	19 ± 7	-	355 ± 53	189 ± 28	10.2

Reaction conditions and detection methods are described in the Online Methods. The concentrations of ADP, GDP, AMP and GMP were calculated by subtracting the values obtained in reactions without phosphate acceptors from those with phosphate acceptors. Kinetic parameters were calculated by fitting kinetic equations to the data shown in **Supplementary Figures 9** and **15** and are shown with the s.d.

that the conversion of nucleosides to R15P occurs through a nucleoside kinase reaction followed by the AMPpase reaction, the discovery of ADP-R1P kinase provides an alternative route through which R15P is generated from nucleosides via the phosphorolysis of nucleosides (generating R1P and base), followed by phosphorylation by ADP-R1P kinase (generating R15P; **Fig. 1b**).

To examine whether such metabolism actually occurs in *T. kodakarensis* cells, we measured the accumulation of R15P when nucleoside substrates with phosphate were added to cell-free extracts in the presence of ADP. In the case of adenosine, guanosine and uridine, but not cytidine, we clearly observed R15P generation in the wild-type *T. kodakarensis* KOD1 strain and the host strain KW128 (**Table 3** and **Supplementary Table 3**). R15P was not formed when ADP was omitted, supporting the involvement of TK2029. Moreover, in the presence of ADP, we clearly observed R15P generation from R1P. This was not observed in the absence of ADP. At present, we cannot provide an explanation for the lack of R15P formation from cytidine. We did not observe R15P formation from cytidine in the presence of either ADP or ATP. As we also could not detect CMP formation from cytidine in the presence of ATP using HPLC, we presumed that its absence was due to insufficient levels of cytidine kinase activity in the cells. This was supported by the fact that we observed R15P generation from CMP in the cell extracts (**Table 3**). We thus examined R15P formation from cytidine using extracts from cells grown in the presence of 10 mM cytidine. However, R15P generation could not be observed. We also performed a DNA microarray analysis to examine whether the transcript levels of cytidine kinase or AMPpase respond to cytidine (**Supplementary Table 4**). We found that the transcript levels of AMPpase moderately but consistently increased in the presence of 10 mM cytidine (1.5-fold). In contrast, those of cytidine kinase (1.0-fold), R15P isomerase (1.1-fold), Rubisco (1.2-fold), ADP-R1P kinase (1.0-fold) and the three nucleoside phosphorylases TK1479 (1.1-fold), TK1482 (1.1-fold) and TK1895 (1.2-fold) showed lower degrees of response. There may be unknown factors that inhibit CMP formation or unidentified growth conditions that induce cytidine kinase activity.

If the formation of R1P and bases from nucleosides and phosphate are dependent on nucleoside phosphorylase reactions, omitting phosphate from the reaction mixture should lead to decreases in R1P generation and, subsequently, in R15P accumulation. As expected, when phosphate was not included, R15P generation decreased to less than 50% of that observed in its presence (**Supplementary Table 5**). Removal of phosphate did not affect R15P generation from R1P, consistent with the assumption that this conversion is catalyzed by ADP-R1P kinase alone and does not involve nucleoside phosphorylases.

Effects of gene disruption on R15P generation

For further confirmation, we constructed gene disruption strains of all of the enzymes presumed to be involved in the conversion from nucleosides and phosphate to R15P; cytidine kinase (TK1843), ADP-R1P kinase (TK2029), the three putative nucleoside phosphorylases (TK1479, TK1482, TK1895) as well as AMPpase (TK0352; **Supplementary Fig. 16** and **Supplementary Table 6**). We first confirmed R15P generation from NMPs and phosphate in cell extracts of the wild-type KOD1 and host KW128 strains, which we presumed was catalyzed by AMPpase. Consistent with the substrate specificity of the recombinant AMPpase[13], we observed R15P accumulation from CMP, AMP and UMP but not GMP (**Table 3** and **Supplementary Table 3**). Disruption of TK0352 led to a complete loss of R15P generation, indicating that AMPpase is responsible for this conversion. We next examined the effects of gene disruption on the conversion of individual nucleosides to R15P. As described above, we observed R15P formation from adenosine, guanosine and uridine with phosphate in the wild-type and host strains. The generation of R15P observed in the host strain was abolished when the *TK2029* gene encoding ADP-R1P kinase was disrupted, but it was not affected by disruption of the gene encoding AMPpase (**Table 3**). This indicated that the conversion of the ribose moieties of adenosine, guanosine and uridine to R15P occurred via the ADP-R1P kinase reaction and not through nucleoside kinase reactions followed by phosphorolysis by AMPpase. We next examined the nucleoside phosphorylase gene disruption strains. In the case of adenosine, we observed a large decrease in R15P generation in cell extracts of the *TK1895* disruption strain, indicating that this gene encodes the major phosphorylase responsible for adenosine phosphorolysis. Disruption of *TK1479* and *TK1482* resulted in a complete loss of R15P generation from uridine and guanosine, respectively. As expected, disruption of the genes encoding the nucleoside phosphorylases had no effect on the conversion from R1P to R15P.

To determine the distribution of the pathway indicated in this study, we examined the presence of homologs of the nucleoside phosphorylases, ADP-R1P kinase, R15P isomerase and Rubisco as well as cytidine kinase and AMPpase. Although the type of nucleoside phosphorylase that is found varies among different organisms, nucleoside phosphorylase homologs were present on every archaeal genome, with the exception of *Nanoarchaeum equitans*. Homologs of each of the three nucleoside phosphorylases were present in all *Thermococcus* species. Notably, however, uridine phosphorylase homologs were not found in the *Pyrococcus* species. ADP-R1P kinase, R15P isomerase and Rubisco homologs were present in single copies throughout members of the *Thermococcus* and *Pyrococcus* species. Homologs of the cytidine kinase were found only in members of the *Thermococcus* species. This suggested that the conversion of adenosine and guanosine to 3-PGA is present throughout the *Thermococcus* and *Pyrococcus* species, whereas the conversion of uridine to 3-PGA may only occur in the *Thermococcus* species. In other archaea, there were many organisms in which we found homologs of nucleoside phosphorylase, R15P isomerase and Rubisco but not ADP-R1P kinase. These included some members of the Desulfurococcales, Archaeoglobales, Halobacteriales, Methanococcales, Methanomicrobiales and Methanosarcinales. We speculated that these organisms might harbor enzymes that use phosphate donors other than ADP for R1P

Table 3 | R15P generation in cell-free extracts of the gene disruption strains

Substrate	Strain						
	KW128 (host)	Δtk0352 (Δampp)	Δtk1479 (Δudp)	Δtk1482 (Δpnp)	Δtk1895 (Δpnp)	Δtk1843 (Δcydk)	Δtk2029 (Δr1pk)
None + ADP	0.07 ± 0.06	0.05 ± 0.03	0.07 ± 0.05	0.05 ± 0.03	0.06 ± 0.02	0.01 ± 0.03	0.08 ± 0.03
None + ATP	0.06 ± 0.04	0.05 ± 0.02	0.04 ± 0.01	0.02 ± 0.02	0.03 ± 0.02	0.03 ± 0.01	0.03 ± 0.01
R1P	0.05 ± 0.02	0.03 ± 0.04	0.02 ± 0.02	0.02 ± 0.05	0.04 ± 0.03	0.04 ± 0.03	0.01 ± 0.05
R1P + ADP	2.70 ± 0.38	3.11 ± 0.23	2.89 ± 0.30	2.52 ± 0.27	2.89 ± 0.25	2.97 ± 0.48	-0.01 ± 0.07
Adenosine	0.01 ± 0.02	0.02 ± 0.01	0.04 ± 0.01	0.02 ± 0.04	0.03 ± 0.03	0.02 ± 0.04	0.08 ± 0.05
Adenosine + ADP	1.45 ± 0.15	1.53 ± 0.07	1.48 ± 0.18	1.15 ± 0.18	0.20 ± 0.05	1.47 ± 0.27	0.03 ± 0.02
Guanosine	0.00 ± 0.04	0.01 ± 0.07	0.03 ± 0.03	-0.01 ± 0.03	0.01 ± 0.03	0.04 ± 0.04	0.01 ± 0.03
Guanosine + ADP	1.20 ± 0.14	1.19 ± 0.12	1.26 ± 0.16	0.03 ± 0.02	1.21 ± 0.13	1.07 ± 0.17	0.07 ± 0.01
Uridine	0.04 ± 0.09	0.02 ± 0.02	0.02 ± 0.00	0.01 ± 0.01	0.03 ± 0.03	0.02 ± 0.04	0.01 ± 0.01
Uridine + ADP	1.25 ± 0.21	1.16 ± 0.10	0.03 ± 0.05	1.09 ± 0.15	1.10 ± 0.10	1.08 ± 0.12	0.01 ± 0.02
Cytidine	0.00 ± 0.02	0.02 ± 0.02	0.02 ± 0.03	0.00 ± 0.04	0.01 ± 0.04	0.03 ± 0.08	0.01 ± 0.05
Cytidine + ADP	0.13 ± 0.02	0.06 ± 0.01	0.05 ± 0.01	0.04 ± 0.04	0.11 ± 0.10	0.03 ± 0.03	0.06 ± 0.05
Cytidine + ATP	0.02 ± 0.02	0.04 ± 0.03	0.04 ± 0.03	0.09 ± 0.02	0.08 ± 0.04	0.05 ± 0.02	0.02 ± 0.04
AMP	0.76 ± 0.11	0.02 ± 0.05	0.73 ± 0.07	0.62 ± 0.08	0.67 ± 0.12	0.60 ± 0.05	0.75 ± 0.19
CMP	2.33 ± 0.28	0.04 ± 0.01	2.34 ± 0.36	2.04 ± 0.17	2.14 ± 0.34	2.11 ± 0.17	2.23 ± 0.43
GMP	0.08 ± 0.02	0.02 ± 0.01	0.11 ± 0.04	0.09 ± 0.05	0.14 ± 0.01	0.08 ± 0.06	0.07 ± 0.01
UMP	0.54 ± 0.11	0.04 ± 0.03	0.56 ± 0.07	0.50 ± 0.04	0.47 ± 0.04	0.56 ± 0.07	0.52 ± 0.08

Reaction conditions and detection methods are described in Online Methods. The units for all values are mM. The data represent the average of three independent experiments from three independent cultures and are shown with the s.d. Abbreviations are as follows: ampp, AMPpase; udp, uridine phosphorylase; pnp, purine nucleoside phosphorylase; cydk, cytidine kinase; r1pk, ADP-R1P kinase.

phosphorylation (for example, ATP) and thus differ from ADP-R1P kinase in primary structure. As most of these organisms also harbored an AMPpase homolog, there is also the possibility that these species harbor multiple nucleoside kinases and do not use the pathway involving R1P formation for nucleoside degradation.

DISCUSSION

The metabolism indicated from our studies is summarized in **Figure 1b**. We show that the previously reported NMP degradation pathway is a portion of a larger metabolic network involved in the conversion and degradation of nucleosides and NMPs. Using phosphate and ADP, the ribose moieties of adenosine, guanosine and uridine are converted to R15P via R1P by nucleoside phosphorylases and ADP-R1P kinase. R15P can be directed to glycolysis via the functions of R15P isomerase and Rubisco. Alternatively, R15P may also be converted to NMPs via the function of AMPpase, recycling the nucleobases that are released in the nucleoside phosphorylase reactions. The fact that cytidine was not recognized by this pathway, as in the case of the other three nucleosides, is intriguing. The distinction between cytidine and other nucleosides, however, is also observed in bacteria and eukaryotes. It is presumed that bacteria and eukaryotes harbor nucleoside phosphorylases that recognize adenosine, guanosine and uridine, but not cytidine. Cytidine is first converted to uridine in these organisms, which is recognized by uridine phosphorylase and then converted to R1P and uracil[34].

The metabolism shown in **Figure 1b** provides a feasible explanation as to why R15P isomerase displays activity only in the presence of AMP accumulation[13]. We can now presume that unless sufficient levels of NMPs (represented by AMP) are available, R15P may be used for NMP synthesis via AMPpase. When AMP is abundant, R15P is directed to glycolysis via the activated R15P isomerase and Rubisco. Another puzzling observation was that R15P isomerase and Rubisco production, but not AMPpase, were induced upon the addition of nucleosides to the medium[13]. This also seems reasonable now, as only R15P isomerase and Rubisco would be required to direct the ribose moieties of excess nucleosides to glycolysis. Nucleoside degradation in bacteria and eukaryotes also occurs by nucleoside phosphorolysis, resulting in R1P and base formation. However, R1P is converted to ribose 5-phosphate (R5P) by phosphoribomutase, R5P is converted to ribulose 5-phosphate (Ru5P) by phosphoriboisomerase, and Ru5P is converted to xylulose 5-phosphate by Ru5P epimerase, all of which are directed to glycolysis via the pentose phosphate pathway[35,36] (**Fig. 1a**). R5P is also converted to phosphoribosylpyrophosphate, leading to NMP synthesis. Although the archaeal genomes harbor nucleoside phosphorylase homologs, enzymes that can further convert their product, R1P, have not been identified. Furthermore, Archaea do not harbor homologs of the phosphoribomutases from Bacteria. In eukaryotes also, the metabolism of R1P had not been understood until recently. In the yeast *Saccharomyces cerevisiae*, it was demonstrated that the phosphoglucomutase 3 of this organism is responsible for R1P conversion (to R5P)[37]. Although the metabolism of R1P generated from the phosphorylases is still unknown in archaea that do not have an ADP-R1P kinase homolog, this study indicates that, at least in *T. kodakarensis* and most likely in all members of the Thermococcales, R1P can be converted to R15P, which acts as a central metabolite that can either be directed to glycolysis or converted to NMPs. When R15P is directed to glycolysis, this form of metabolism substitutes for the pentose phosphate pathway, which directs R1P to glycolysis via R5P. Although energy is consumed in the pathway in *T. kodakarensis*, six molecules of 3-PGA are produced from three molecules of R1P owing to the carboxylase reaction of Rubisco, whereas only five 3-PGA molecules are produced from the pentose phosphate pathway. In contrast, the route from R1P to NMPs via R15P can function as a pathway for nucleoside salvage, which in bacteria and eukaryotes is carried out by converting R1P to NMPs via R5P and phosphoribosylpyrophosphate, as described above.

Our results reveal the presence of a previously unidentified metabolic network in the Thermococcales. In the classical pentose phosphate pathway, the R1P generated from nucleosides is converted to intermediates of glycolysis and gluconeogenesis via the monophosphates R5P, Ru5P and xylulose 5-phosphate (**Fig. 1a**). In the pathway identified in this study, R1P is directed toward central

carbon metabolism via R15P and RuBP, which are both bisphosphate compounds (**Fig. 1b**). We therefore designate this metabolic route as the pentose bisphosphate pathway.

Received 5 August 2014; accepted 27 February 2015; published online 30 March 2015

METHODS

Methods and any associated references are available in the online version of the paper.

References

1. Wamelink, M.M., Struys, E.A. & Jakobs, C. The biochemistry, metabolism and inherited defects of the pentose phosphate pathway: a review. *J. Inherit. Metab. Dis.* **31**, 703–717 (2008).
2. Riganti, C., Gazzano, E., Polimeni, M., Aldieri, E. & Ghigo, D. The pentose phosphate pathway: an antioxidant defense and a crossroad in tumor cell fate. *Free Radic. Biol. Med.* **53**, 421–436 (2012).
3. Soderberg, T. Biosynthesis of ribose-5-phosphate and erythrose-4-phosphate in archaea: a phylogenetic analysis of archaeal genomes. *Archaea* **1**, 347–352 (2005).
4. Orita, I. *et al.* The ribulose monophosphate pathway substitutes for the missing pentose phosphate pathway in the archaeon. *Thermococcus kodakaraensis*. *J. Bacteriol.* **188**, 4698–4704 (2006).
5. Ezaki, S., Maeda, N., Kishimoto, T., Atomi, H. & Imanaka, T. Presence of a structurally novel type ribulose-bisphosphate carboxylase/oxygenase in the hyperthermophilic archaeon, *Pyrococcus kodakaraensis* KOD1. *J. Biol. Chem.* **274**, 5078–5082 (1999).
6. Finn, M.W. & Tabita, F.R. Synthesis of catalytically active form III ribulose 1,5-bisphosphate carboxylase/oxygenase in archaea. *J. Bacteriol.* **185**, 3049–3059 (2003).
7. Watson, G.M., Yu, J.P. & Tabita, F.R. Unusual ribulose 1,5-bisphosphate carboxylase/oxygenase of anoxic *Archaea*. *J. Bacteriol.* **181**, 1569–1575 (1999).
8. Kitano, K. *et al.* Crystal structure of a novel-type archaeal rubisco with pentagonal symmetry. *Structure* **9**, 473–481 (2001).
9. Alonso, H., Blayney, M.J., Beck, J.L. & Whitney, S.M. Substrate-induced assembly of *Methanococcoides burtonii* D-ribulose-1,5-bisphosphate carboxylase/oxygenase dimers into decamers. *J. Biol. Chem.* **284**, 33876–33882 (2009).
10. Sato, T., Atomi, H. & Imanaka, T. Archaeal type III RuBisCOs function in a pathway for AMP metabolism. *Science* **315**, 1003–1006 (2007).
11. Nakamura, A. *et al.* Dynamic, ligand-dependent conformational change triggers reaction of ribose-1,5-bisphosphate isomerase from *Thermococcus kodakarensis* KOD1. *J. Biol. Chem.* **287**, 20784–20796 (2012).
12. Nishitani, Y. *et al.* Structure analysis of archaeal AMP phosphorylase reveals two unique modes of dimerization. *J. Mol. Biol.* **425**, 2709–2721 (2013).
13. Aono, R. *et al.* Enzymatic characterization of AMP phosphorylase and ribose-1,5-bisphosphate isomerase functioning in an archaeal AMP metabolic pathway. *J. Bacteriol.* **194**, 6847–6855 (2012).
14. Hansen, T., Arnfors, L., Ladenstein, R. & Schönheit, P. The phosphofructokinase-B (MJ0406) from *Methanocaldococcus jannaschii* represents a nucleoside kinase with a broad substrate specificity. *Extremophiles* **11**, 105–114 (2007).
15. Elkin, S.R., Kumar, A., Price, C.W. & Columbus, L. A broad specificity nucleoside kinase from *Thermoplasma acidophilum*. *Proteins* **81**, 568–582 (2013).
16. Park, J. & Gupta, R.S. Adenosine kinase and ribokinase—the RK family of proteins. *Cell. Mol. Life Sci.* **65**, 2875–2896 (2008).
17. Kengen, S.W. *et al.* Evidence for the operation of a novel Embden-Meyerhof pathway that involves ADP-dependent kinases during sugar fermentation by *Pyrococcus furiosus*. *J. Biol. Chem.* **269**, 17537–17541 (1994).
18. Kengen, S.W., Tuininga, J.E., de Bok, F.A., Stams, A.J. & de Vos, W.M. Purification and characterization of a novel ADP-dependent glucokinase from the hyperthermophilic archaeon *Pyrococcus furiosus*. *J. Biol. Chem.* **270**, 30453–30457 (1995).
19. Tuininga, J.E. *et al.* Molecular and biochemical characterization of the ADP-dependent phosphofructokinase from the hyperthermophilic archaeon *Pyrococcus furiosus*. *J. Biol. Chem.* **274**, 21023–21028 (1999).
20. Sakuraba, H. *et al.* ADP-dependent glucokinase/phosphofructokinase, a novel bifunctional enzyme from the hyperthermophilic archaeon *Methanococcus jannaschii*. *J. Biol. Chem.* **277**, 12495–12498 (2002).
21. Guixé, V. & Merino, F. The ADP-dependent sugar kinase family: kinetic and evolutionary aspects. *IUBMB Life* **61**, 753–761 (2009).
22. Merino, F., Rivas-Pardo, J.A., Caniuguir, A., García, I. & Guixé, V. Catalytic and regulatory roles of divalent metal cations on the phosphoryl-transfer mechanism of ADP-dependent sugar kinases from hyperthermophilic archaea. *Biochimie* **94**, 516–524 (2012).
23. Castro-Fernandez, V., Bravo-Moraga, F., Herrera-Morande, A. & Guixe, V. Bifunctional ADP-dependent phosphofructokinase/glucokinase activity in the order Methanococcales—biochemical characterization of the mesophilic enzyme from *Methanococcus maripaludis*. *FEBS J.* **281**, 2017–2029 (2014).
24. Ronimus, R.S. & Morgan, H.W. Cloning and biochemical characterization of a novel mouse ADP-dependent glucokinase. *Biochem. Biophys. Res. Commun.* **315**, 652–658 (2004).
25. Marbaix, A.Y. *et al.* Extremely conserved ATP- or ADP-dependent enzymatic system for nicotinamide nucleotide repair. *J. Biol. Chem.* **286**, 41246–41252 (2011).
26. Kengen, S.W. *et al.* ADP-dependent glucokinase and phosphofructokinase from *Pyrococcus furiosus*. *Methods Enzymol.* **331**, 41–53 (2001).
27. Boyer, P.D. & Robbins, E.A. Determination of the equilibrium of the hexokinase reaction and the free energy of hydrolysis of adenosine triphosphate. *J. Biol. Chem.* **224**, 121–135 (1957).
28. Minakami, S. & Yoshikawa, H. Thermodynamic considerations on erythrocyte glycolysis. *Biochem. Biophys. Res. Commun.* **18**, 345–349 (1965).
29. Cacciapuoti, G., Bertoldo, C., Brio, A., Zappia, V. & Porcelli, M. Purification and characterization of 5′-methylthioadenosine phosphorylase from the hyperthermophilic archaeon *Pyrococcus furiosus*: substrate specificity and primary structure analysis. *Extremophiles* **7**, 159–168 (2003).
30. Cacciapuoti, G. *et al.* Biochemical and structural characterization of mammalian-like purine nucleoside phosphorylase from the Archaeon *Pyrococcus furiosus*. *FEBS J.* **274**, 2482–2495 (2007).
31. Cacciapuoti, G., Porcelli, M., Bertoldo, C., De Rosa, M. & Zappia, V. Purification and characterization of extremely thermophilic and thermostable 5-methylthioadenosi 5(-methylthioadenosine phosphorylase from the archaeon *Sulfolobus solfataricus*. Purine nucleoside phosphorylase activity and evidence for intersubunit disulfide bonds. *J. Biol. Chem.* **269**, 24762–24769 (1994).
32. Cacciapuoti, G. *et al.* A novel hyperthermostable 5-deoxy-5-methylthioadenosi phosphorylase from the archaeon *Sulfolobus solfataricus*. *FEBS J.* **272**, 1886–1899 (2005).
33. Fukui, T. *et al.* Complete genome sequence of the hyperthermophilic archaeon *Thermococcus kodakaraensis* KOD1 and comparison with *Pyrococcus* genomes. *Genome Res.* **15**, 352–363 (2005).
34. Ipata, P.L., Camici, M., Micheli, V. & Tozz, M.G. Metabolic network of nucleosides in the brain. *Curr. Top. Med. Chem.* **11**, 909–922 (2011).
35. Tozzi, M.G., Camici, M., Mascia, L., Sgarrella, F. & Ipata, P.L. Pentose phosphates in nucleoside interconversion and catabolism. *FEBS J.* **273**, 1089–1101 (2006).
36. Camici, M., Tozzi, M.G. & Ipata, P.L. Methods for the determination of intracellular levels of ribose phosphates. *J. Biochem. Biophys. Methods* **68**, 145–154 (2006).
37. Walther, T. *et al.* The *PGM3* gene encodes the major phosphoribomutase in the yeast *Saccharomyces cerevisiae*. *FEBS Lett.* **586**, 4114–4118 (2012).

Acknowledgments

This study was funded by the Core Research for Evolutional Science and Technology program of the Japan Science and Technology Agency to H.A. within the research area 'Creation of Basic Technology for Improved Bioenergy Production through Functional Analysis and Regulation of Algae and Other Aquatic Microorganisms'. R.A. is a Research Fellow of the Japan Society for the Promotion of Science.

Author contributions

H.A., T.I., T.S. and R.A. designed the work; R.A. carried out the experiments; R.A., T.S. and H.A. wrote the manuscript.

Competing financial interests

The authors declare no competing financial interests.

Additional information

Supplementary information is available in the online version of the paper. Reprints and permissions information is available online at http://www.nature.com/reprints/index.html. Correspondence and requests for materials should be addressed to H.A.

ONLINE METHODS

Strains and culture conditions. *E. coli* strains DH5α (Takara, Ohtsu, Japan) and BL21-CodonPlus (DE3)-RIL (Agilent Technologies, Santa Clara, CA) were used for plasmid construction and heterologous gene expression, respectively. These strains were cultivated at 37 °C in Luria-Bertani (LB) medium containing 100 μg/ml ampicillin (Nacalai Tesque, Kyoto, Japan)[38]. *T. kodakarensis* KOD1 (refs. 33,39) was cultivated under strictly anaerobic conditions at 85 °C in a growth medium based on artificial sea water (ASW)[40]. Briefly, the nutrient-rich ASW-YT-S^0 medium was composed of 0.8× ASW, 0.5% yeast extract (Nacalai Tesque), 0.5% tryptone (Nacalai Tesque) and 0.2% elemental sulfur. The minimal ASW-AA-S^0 medium was composed of 0.8× ASW, 20 amino acids, trace vitamins, minerals and 0.2% elemental sulfur.

Chemicals and enzymes used for coupling reactions. The sources and purities of the chemicals used in this study are as follows. Adenosine (≥99%), cytidine (≥99%), guanosine (98%), uridine (≥99%), inosine (≥99%), xanthosine (≥99%), deoxyadenosine (99–100%), deoxycytidine (≥99%), deoxyguanosine (≥99–100%), deoxyuridine (99–100%), deoxythymidine (≥99%), deoxyribose 1-phosphate (dR1P, ≥97%), ribose 5-phosphate (≥99%), glucose 1-phosphate (98–99%), glucose 6-phosphate (≥98%), fructose 6-phosphate (≥98%), ribose (≥99%), fructose (≥99%), xylose (≥99%), erythrose (≥75%), glucose (≥99.5%), D-arabinose (≥98%), L-arabinose (≥99%), lyxose (99%), ribulose (≥97.0%), xylulose (≥98%), erythrulose (≥85%), deoxyribose (≥99.0%), gluconate (49–53 wt. % in H_2O), ADP (≥95%), CDP (≥95%), GDP (≥96%), UDP (≥96.0%), CTP (≥95%), GTP (≥95%), UTP (≥96%), AMP (≥99%), CMP (≥99%), GMP (≥99%), UMP (≥99%) and pyrophosphate (≥99%) were purchased from Sigma-Aldrich (St. Louis, USA). Ribose 1-phosphate (R1P, 98%) was purchased from Toronto Research Chemicals Inc. (Toronto, Canada). ATP (≥95%) and NADH (≥95%) were purchased from Oriental Yeast (Tokyo, Japan). Phosphoenolpyruvate (PEP, ≥98.0%) was purchased from Wako Pure Chemical Industries, Ltd. (Osaka, Japan). Ribose 1,5-bisphosphate (R15P, ≥98.0%) was purchased from Tokyo Chemical Industry Co., Ltd. (Tokyo, Japan).

The sources of the enzymes used in this study are as follows. Pyruvate kinase/lactic dehydrogenase enzymes from rabbit muscle (PK/LDH), 3-phosphoglyceric phosphokinase from baker's yeast, glyceraldehyde-3-phosphate dehydrogenase from rabbit muscle, triosephosphate isomerase from baker's yeast and α-glycerophosphate dehydrogenase from rabbit muscle were purchased from Sigma-Aldrich.

Recombinant AMPpase, ribose-1,5-bisphosphate isomerase (R15P isomerase) and type III ribulose-1,5-bisphosphate carboxylase/oxygenase (Rubisco) from *T. kodakarensis* were prepared as follows[13]. For AMPpase, BL21-CodonPlus (DE3)-RIL *E. coli* cells transformed with the expression plasmid pET-*deoA*[10] were grown at 37 °C in LB medium containing 100 μg/ml ampicillin until their optical density at 660 nm reached 0.4–0.8, and gene expression was induced by the addition of 0.1 mM isopropyl-1-thio-β-D-thiogalactopyranoside (IPTG; Nacalai Tesque). Cells were cultured for a further 4 h at 37 °C and then harvested by centrifugation (5,000*g*, 15 min, 4 °C), washed with 1% NaCl in 50 mM Tris(hydroxymethyl)aminomethane (Tris)-HCl (pH 8.0) and collected by centrifugation (5,000*g*, 15 min, 4 °C). Cells were resuspended in 50 mM Tris-HCl (pH 7.5) and disrupted by sonication. Soluble proteins were incubated for 10 min at 80 °C and centrifuged (20,000*g*, 30 min, 4 °C) to remove thermolabile proteins deriving from the host cells. The supernatant was applied to an anion exchange column Resource Q (GE Healthcare, Little Chalfont, Buckinghamshire, UK), and proteins were eluted with a linear gradient of NaCl (0–1.0 M) in 50 mM Tris-HCl (pH 7.5). After the fractions containing AMPpase were concentrated with an Amicon Ultra centrifugal filter unit (MWCO 100,000; Millipore, Billerica, MA), the sample was applied to a gel filtration column Superdex 200 (GE Healthcare) with a mobile phase of 150 mM NaCl in 50 mM Tris-HCl (pH 7.5).

For R15P isomerase, after the expression plasmid (pCold-His-e2b2 (ref. 11)) was introduced into BL21-CodonPlus (DE3)-RIL, cells were grown at 37 °C in LB medium containing 100 μg/ml ampicillin until their optical density at 660 nm reached 0.4–0.8. IPTG (0.1 mM) was added, followed by further incubation at 15 °C for 40 h. Cells were harvested by centrifugation (5,000*g*, 15 min, 4 °C), washed with 1% NaCl in 50 mM Tris-HCl (pH 8.0) and collected by centrifugation (5,000*g*, 15 min, 4 °C). The harvested cells were resuspended in 20 mM sodium phosphate (pH 7.4) containing 500 mM NaCl and 40 mM imidazole and disrupted by sonication. The crude extract was heat-treated for 30 min at 85 °C, cooled on ice and then centrifuged (20,000*g*, 30 min, 4 °C). The supernatant was applied to a Ni^{2+} column, His GraviTrap (GE Healthcare), and the R15P isomerase protein was eluted with 20 mM sodium phosphate (pH 7.4) containing 500 mM NaCl and 500 mM imidazole. The buffer was exchanged to 100 mM *N*,*N*-bis(2-hydroxyethyl)glycine (Bicine)-NaOH (pH 8.3) containing 10 mM $MgCl_2$ and 1.2 M $(NH_4)_2SO_4$ using a PD-10 column (GE Healthcare). The protein solution containing the R15P isomerase protein was loaded onto a hydrophobic interaction column, Resource ISO (GE Healthcare), and then eluted with a linear gradient of $(NH_4)_2SO_4$ concentration from 1.2 M to 0 M. The concentration of $(NH_4)_2SO_4$ in the fractions containing R15P isomerase protein was reduced by ultrafiltration with 100 mM Bicine-NaOH (pH 8.3), 10 mM $MgCl_2$ and 100 mM NaCl using an Amicon Ultra centrifugal filter unit (MWCO 10,000; Millipore).

For Rubisco, *E. coli* BL21-CodonPlus (DE3)-RIL cells were transformed with a previously described expression plasmid[5], and gene expression was performed in the same way as for AMPpase. Cells were resuspended in 100 mM Bicine-NaOH (pH 8.3) containing 10 mM $MgCl_2$ and disrupted by sonication. Soluble proteins were incubated for 30 min at 85 °C and centrifuged (20,000*g*, 30 min, 4 °C). The supernatant was applied to Resource Q, and proteins were eluted with a linear gradient of NaCl (0–1.0 M) in 100 mM Bicine-NaOH (pH 8.3) containing 10 mM $MgCl_2$. $(NH_4)_2SO_4$ was added to the fractions containing the recombinant Rubisco protein at a final concentration of 1.2 M. The protein solution was applied to a hydrophobic interaction column Resource PHE (GE Healthcare), and proteins were eluted with a linear gradient of $(NH_4)_2SO_4$ (1.2–0 M) in 100 mM Bicine-NaOH (pH 8.3) and 10 mM $MgCl_2$. The fractions containing the recombinant Rubisco were concentrated using an Amicon Ultra centrifugal filter unit (MWCO 30,000) and further purified by Superdex 200 with a mobile phase of 100 mM Bicine-NaOH (pH 8.3), 10 mM $MgCl_2$ and 100 mM NaCl.

Preparation of the TK1843 and TK2029 proteins. Plasmids for gene expression of TK1843 and TK2029 in *E. coli* were constructed as follows. The coding region of each gene was amplified from the genomic DNA of *T. kodakarensis* KOD1 by PCR using the primer sets TK1843f-TK1843r and TK2029f-TK2029r for TK1843 and TK2029, respectively (**Supplementary Table 7**). After digestion with NdeI (Takara) and BamHI (Toyobo, Osaka, Japan), the fragments were individually inserted into pET-21a (+) (Novagen, Madison, WI) digested with the same restriction enzymes.

BL21 CodonPlus (DE3)-RIL *E. coli* competent cells were transformed with each recombinant plasmid, and gene expression was carried out as in the case of AMPpase. Cells were harvested by centrifugation (5,000*g*, 15 min, 4 °C), washed with 1% NaCl in 50 mM Tris-HCl (pH 8.0) and collected by centrifugation (5,000*g*, 15 min, 4 °C).

To purify the recombinant TK1843 and TK2029 proteins, the harvested cells were resuspended in 50 mM Tris-HCl (pH 7.5) and disrupted by sonication. Soluble proteins were incubated for 30 min at 85 °C and centrifuged (20,000*g*, 30 min, 4 °C). The supernatant was applied to Resource Q, and proteins were eluted with a linear gradient of NaCl (0–1.0 M) in 50 mM Tris-HCl (pH 7.5). $(NH_4)_2SO_4$ was added at a final concentration of 1.5 M to the fractions containing each recombinant protein. The protein solutions were applied to a Resource PHE column, and the proteins were eluted with a linear gradient of $(NH_4)_2SO_4$ (1.5–0 M) in 50 mM Tris-HCl (pH 7.5). After concentrating the fractions containing the TK1843 protein or the TK2029 protein with Amicon Ultra centrifugal filter unit (MWCO 10,000), the samples were applied to Superdex 200 and separated with a mobile phase of 150 mM NaCl in 50 mM Tris-HCl (pH 7.5). The purities of the proteins were confirmed by SDS-PAGE followed by staining with Coomassie Brilliant Blue (**Supplementary Fig. 1**).

Identifying the substrates of TK1843 and TK2029 proteins. To identify candidate compounds that are phosphorylated by the recombinant TK1843 and TK2029 proteins (**Table 1**), reactions were performed in a solution (100 μl) containing 100 mM Tris-HCl (pH 6.7), 10 mM $MgCl_2$, 1.6 μM of the purified TK1843 protein or TK2029 protein, 10 mM substrate and 5 mM ATP or ADP. After preincubation at 85 °C for 3 min, the reaction was initiated by adding substrate and ATP or ADP. The reaction was carried out at 85 °C for 5 min and terminated by rapid cooling on ice for 5 min, and proteins were removed with an Amicon Ultra centrifugal filter unit (MWCO 10,000).

ADP generation from ATP was measured by coupling reactions with PK/LDH. The PK/LDH reaction mixture contained 100 mM Tris-HCl (pH 7.4), 10 mM $MgCl_2$, 0.2 mM NADH, 5 mM phosphoenolpyruvate, 60–100 units ml^{-1}/90–140 units ml^{-1} of PK/LDH from rabbit muscle and an aliquot of the kinase reaction mixture. After preincubation at 42 °C for 2 min, the reaction

was initiated with the addition of an aliquot of the kinase reaction mixture. The decrease in absorbance at 340 nm due to the consumption of NADH was measured.

AMP generation from ADP was measured with HPLC. An aliquot of the kinase reaction mixture was applied to a C_{18} column, COSMOSIL $5C_{18}$-PAQ (Nacalai Tesque), and compounds were separated with 50 mM NaH_2PO_4 (pH 4.3) as the mobile phase. Column temperatures were set at 40 °C, and AMP was detected with a UV detector (A_{254}). The concentrations of AMP were determined with a standard curve generated with defined concentrations of AMP.

Analysis of the reaction products. When detecting CMP generation with HPLC, the reaction mixture (100 µl) was composed of 100 mM Tris-HCl (pH 6.7), 10 mM $MgCl_2$, 1.6 µM of the purified TK1843 protein, 5 mM ATP and 5 mM cytidine. After preincubation at 85 °C for 3 min, the reaction was initiated by adding ATP and cytidine. The reaction was carried out for 5 min at 85 °C, terminated by rapid cooling on ice for 5 min, and the enzymes were removed with an Amicon Ultra centrifugal filter unit (MWCO 10,000). The aliquot of the kinase reaction mixture was monitored by HPLC with methods similar to those used for monitoring AMP, as described above. CMP generation from the TK1843 reaction was also confirmed by a coupling reaction with the purified AMPpase. The reaction mixture (100 µl) was composed of 100 mM Tris-HCl (pH 6.7), 10 mM $MgCl_2$, 1.6 µM of the purified TK1843 protein, 0.93 µM of purified AMPpase, 20 mM sodium phosphate, 5 mM ATP and 20 mM cytidine. After preincubation at 85 °C for 3 min, the reaction was initiated by adding ATP and cytidine. The reaction was carried out for 5 min at 85 °C and terminated by rapid cooling on ice for 5 min, and the enzymes were removed with Amicon Ultra centrifugal filter unit (MWCO 10,000). The R15P generated in the reaction was quantified as described below.

R15P generation was measured with coupling reactions using R15P isomerase and Rubisco. The R15P isomerase–Rubisco reaction mixture (100 µl) was composed of 100 mM Tris-HCl (pH 6.7), 10 mM $MgCl_2$, 1.3 µM of purified R15P isomerase, 1.0 µM of purified Rubisco, 10 mM AMP, 100 mM $NaHCO_3$ and an aliquot of the sample. After preincubation at 85 °C for 3 min, the reaction was initiated by adding $NaHCO_3$ and the sample. The reaction was carried out for 10 min at 85 °C and terminated by rapid cooling on ice for 5 min, and the enzymes were removed with Amicon Ultra centrifugal filter unit (MWCO 30,000). The amount of 3-PGA synthesized by this coupling reaction was determined by a second coupling reaction described elsewhere[13]. The reaction mixture (100 µl) was composed of 100 mM Bicine-NaOH (pH 8.3), 10 mM $MgCl_2$, 5 mM ATP, 0.2 mM NADH, a 20 µl aliquot of the first coupling reaction and 20 µl of the coupling enzymes solution. The coupling enzymes solution contained 563 units ml^{-1} 3-phosphoglycerate phosphokinase, 125 units ml^{-1} glyceraldehyde-3-phosphate dehydrogenase, 260 units ml^{-1} triose-phosphate isomerase, 22.5 units ml^{-1} glycerophosphate dehydrogenase, 5 mM reduced glutathione, 0.1 mM EDTA and 20% glycerol in 50 mM Bicine-NaOH (pH 8.0). The assay mixture without the coupling enzymes solution was preincubated at 25 °C for 3 min, and the reaction was initiated with the addition of the coupling enzymes solution. The difference in absorbance at 340 nm due to the conversion of NADH into NAD^+ by the coupling reaction was measured.

Biochemical analysis of cytidine kinase. Standard activity measurements were carried out for the TK1843 protein as follows. The reaction mixture contained 100 mM *N*-[Tris(hydroxymethyl)methyl]glycine (Tricine)-NaOH (pH 9.0), 10 mM $MgCl_2$, 300 mM KCl, 10 mM cytidine, 5 mM ATP and 8.0–32 nM of the purified TK1843 protein. After preincubation at 85 °C for 3 min, the reaction was initiated by adding ATP. The reaction was carried out at 85 °C for 3 min, 5 min or 7 min and terminated by rapid cooling on ice for 5 min, and proteins were removed with an Amicon Ultra centrifugal filter unit (MWCO 10,000). The kinase activity of TK1843 was measured by monitoring ADP generation from ATP by coupling reactions with PK/LDH as described above. To examine the effects of pH, the following buffers at various pH values were used instead of Tricine-NaOH (pH 9.0): acetate-NaOH (pH 4.0 to 5.5), 2-morpholinoethanesulfonic acid (MES)-NaOH (pH 5.5 to 7.0), 4-(2-hydroxyethyl)-1-piperazineethanesulfonic acid (HEPES)-NaOH (pH 7.0 to 8.0), Tricine-NaOH (pH 8.0 to 9.0) and *N*-cyclohexyl-2-aminoethanesulfonic acid (CHES)-NaOH (pH 9.0 to 10.0). Tris, Bicine, Tricine, MES, HEPES and CHES were obtained from Nacalai Tesque. To examine the effects of temperature, the reaction was performed at various temperature (50 to 95 °C). The data were also used to make an Arrhenius plot for calculating the activation energy. To examine the effects of KCl, the reaction was performed with various concentrations of KCl (0–500 mM). To examine the substrate specificities for phosphate donors, the reaction was performed with 5 mM CTP, GTP or UTP instead of 5 mM ATP. Activity levels with various divalent metal cations were examined by measuring activity in the presence of 15 mM ATP and 30 mM $MgCl_2$, $MnCl_2$, $CaCl_2$, $CoCl_2$, $NiCl_2$, $ZnCl_2$ or $CuCl_2$. Kinetic analyses were performed toward cytidine and deoxycytidine as phosphate acceptors and ATP and GTP as phosphate donors. Concentrations of cytidine and deoxycytidine were varied from 0–20 mM in the presence of a constant concentration of ATP (15 mM) and $MgCl_2$ (30 mM). Concentrations of ATP and GTP were varied from 0–30 mM in the presence of a constant concentration of cytidine (10 mM) and $MgCl_2$ (30 mM).

Biochemical analysis of ADP-dependent R1P kinase. Standard activity measurements were carried out for the TK2029 protein as follows. The reaction mixture contained 100 mM Tricine-NaOH (pH 8.0), 10 mM $MgCl_2$, 10 mM KCl, 5 mM R1P, 5 mM ADP and 1.6–16 nM of the purified TK2029 protein. After preincubation at 85 °C for 3 min, the reaction was initiated by adding ADP. The reaction was carried out at 85 °C for 3 min, 5 min or 7 min and terminated by rapid cooling on ice for 5 min, and proteins were removed with an Amicon Ultra centrifugal filter unit (MWCO 10,000). Kinase activity of TK2029 was measured by monitoring AMP generation with HPLC or, for examining the substrate specificity for phosphate donor, by monitoring R15P generation by the coupling reaction with R15P isomerase and Rubisco, as described above. To examine the effects of pH, the following buffers at various pH values were used instead of Tricine-NaOH (pH 8.0): acetate-NaOH (pH 4.0 to 5.5), MES-NaOH (pH 5.5 to 7.0), HEPES-NaOH (pH 7.0 to 8.0) and Tricine-NaOH (pH 8.0 to 9.0). To examine the effects of temperature, the reaction was performed at various temperatures (30–95 °C). The data were also used to make an Arrhenius plot for calculating the activation energy. To examine the effects of KCl, the reaction was performed with various concentrations of KCl (0–20 mM). To examine the substrate specificities for phosphate donors, the reaction was performed with 5 mM CDP, GDP, UDP or pyrophosphate, instead of 5 mM ADP. Activity levels with various divalent metal cations were examined by measuring activity in the presence of 40 mM ADP and 60 mM $MgCl_2$, $MnCl_2$, $CaCl_2$, $CoCl_2$, $NiCl_2$, $ZnCl_2$ or $CuCl_2$. Kinetic analyses were performed toward R1P and dR1P as phosphate acceptors and ADP and GDP as phosphate donors. Concentrations of R1P and dR1P were varied from 0–15 mM in the presence of a constant concentration of ADP (50 mM) and $MgCl_2$ (60 mM). Concentrations of ADP and GDP were varied from 0–60 mM in the presence of a constant concentration of R1P (5 mM) and $MgCl_2$ (60 mM) or $CaCl_2$ (60 mM).

R15P synthesis from nucleosides in cell-free extract. Cell-free extracts (CFEs) of *T. kodakarensis* were prepared as follows. Cells cultivated in ASW-YT-S^0 medium for 14 h were harvested by centrifugation (5,000*g*, 15 min, 4 °C), washed with 0.8× ASW and centrifuged again (5,000*g*, 15 min, 4 °C). The harvested cells were lysed in 50 mM Tris-HCl (pH 7.5) containing 0.1% Triton X-100 (Nacalai Tesque) at a volume of 1/500 of the culture. After mixing with a vortex for 30 min, the supernatant after centrifugation (20,000*g*, 30 min, 4 °C) was used as the CFE. The first reaction (conversion of nucleosides in CFE) was performed in a mixture (100 µl) containing 100 mM Tris-HCl (pH 6.7), 10 mM $MgCl_2$, CFE (corresponding to 100 µg protein), 20 mM sodium phosphate (pH 7.6), 100 mM $NaHCO_3$, 20 mM nucleoside and 5 mM ATP or ADP. After preincubation at 85 °C for 3 min, the reaction was initiated by adding substrates, sodium phosphates, $NaHCO_3$, nucleoside and ATP or ADP. The reaction was carried out at 85 °C for 30 min and terminated by rapid cooling on ice for 5 min, and proteins were removed with an Amicon Ultra centrifugal filter unit (MWCO 3,000; Millipore). The R15P generated from the nucleosides was then measured by the coupling reactions with R15P isomerase and Rubisco as described above. The $NaHCO_3$ in the reaction mixture is to ensure that even if small fractions of R15P were converted to the thermolabile RuBP by R15P isomerase, the RuBP would be converted to 3-PGA by Rubisco and thus included in our calculations.

DNA microarray analysis. *T. kodakarensis* KOD1 was cultivated at 85 °C in ASW-YT-Pyr with or without 10 mM cytidine. Cells were harvested in the early log phase (optical density at 660 nm of 0.2–0.3), and total RNA was extracted using the RNeasy Midi kit (Qiagen, Venlo, The Netherlands). The experimental procedures taken for microarray analysis were as described elsewhere[41,42].

doi:10.1038/nchembio.1786

The microarray plate used in this study (Array Tko2) was obtained from Takara, which covers all 2,306 genes of *T. kodakarensis* KOD1. As two identical sets (left and right) were loaded on each plate, two sets of data are obtained from each microarray plate.

Fluorescently labeled cDNA used for hybridization was prepared from the RNA extracted above using the RNA Fluorescence Labeling Core kit version 2.0 (Takara). Total RNA (15 μg) was annealed with random hexamers, and reverse transcription was performed in the reaction mixture containing CyDye-labeled dUTP (Cy3-dUTP or Cy5-dUTP; GE Healthcare). After degradation of RNA with RNase H, the labeled cDNA was purified using a column supplied in the kit according to the manufacturer's instructions. The labeled cDNA was dissolved in hybridization buffer (40 μl) containing 6× SSC (1× SSC is 0.15 M NaCl, 0.015 M sodium citrate), 0.2% SDS, 5× Denhardt's solution (Sigma-Aldrich) and 0.1 mg/ml denatured salmon sperm DNA. Hybridization was performed under a coverslip (Spaced Cover Glass XL, Takara) in a humidity chamber at 65 °C for 12–15 h. After hybridization, the microarray plates were washed four times with 2× SSC and 0.2% SDS at 55 °C for 5 min, rinsed in 0.05× SSC and dried by centrifugation. The intensities of the Cy3 and Cy5 dyes were measured by using an Affymetrix 428 Array Scanner (Affymetrix, Santa Clara, CA). The microarray images were analyzed using ImaGene version 5.5 software (BioDiscovery, Marina Del Ray, CA).

Construction of the gene disruption vectors. Plasmids for the disruption of TK0352, TK1843, TK2029, TK1479, TK1482 and TK1895 genes in *T. kodakarensis* using double-crossover homologous recombination were constructed as follows. DNA fragments containing the target gene together with its flanking regions (approximately 1,000 bp each) were amplified from *T. kodakarensis* KOD1 genomic DNA using the primer sets TK0352u900f-TK0352d900r, TK1843u1000f-TK1843d1000r, TK2029u1000f-TK2029d1000r, TK1479u1000f-TK1479d1000r, TK1482u1000f-TK1482d1000r and TK1895u1000f-TK1895d1000r (**Supplementary Table 7**). The amplified DNA fragments were inserted into pUC118 (Takara) digested with HincII (Toyobo). Inverse PCR reactions were carried out to amplify the flanking regions and the pUC118 backbone, thereby removing almost all of the coding regions (not any part of the flanking coding regions) using the primer sets TK0352d1f-TK0352u1r, TK1843-827f-TK1843u1r, TK2029-872f-TK2029u1r, TK1479d1f-TK1479u1r, TK1482d1f-TK1482u1r and TK1895d1f-TK1895u1r (**Supplementary Table 7**). The amplified DNA fragments were ligated with the *trpE* marker cassette and excised from pUMT2 (ref. 43) with PvuII (Toyobo). The marker cassette was oriented so that it would be transcribed in the same direction as the target gene. The constructed plasmids were sequenced to confirm the absence of unintended mutations.

Transformation of *T. kodakarensis*. Transformation of *T. kodakarensis* KW128 with the *trpE* marker was performed as described previously[43] with some modifications. With *trpE* as a selectable marker, transformation was performed as follows. After cultivation of the host strain in ASW-YT-S^0 medium, cells were harvested from 3 ml of the medium (20,000*g*, 5 min, 4 °C), and resuspended in 200 μl of 0.8× ASW. After 3 μg of the plasmid constructed above was added into the suspension, the cells were incubated on ice for 1.5 h. *trpE*$^+$ strains displaying tryptophan prototrophy were selected by cultivating the cells twice in ASW-AA-S^0 medium without tryptophan before spreading them onto ASW-AA solid medium without tryptophan or ASW-YT solid medium. After cultivation for 2–5 d at 85 °C, tryptophan prototrophs were isolated and cultivated in ASW-YT-S^0 medium. The genotypes were analyzed by PCR using primer sets annealing outside of the homologous regions (amppase-out-f/amppase-out-r, TK1843u1100f/TK1843d1100r, TK2029u1100f/TK2029d1100r, TK1479u1100f/TK1479d1100r, TK1482u1100f/TK1482d1100r, and TK1895u1100f/TK1895d1100r) and inside of the target gene (amppase-in-f/amppase-in-r, TK1843f/TK1843r, TK2029f/TK2029r, udp-f/udp-r, mtap1-f/mtap1-r, and mtap2-f/mtap2-r; **Supplementary Table 7**). The genotypes were also confirmed by sequencing each locus.

38. Sambrook, J. & Russel, D. *Molecular Cloning: a Laboratory Manual* (Cold Spring Harbor Laboratory Press, Cold Spring Harbor, NY, 2001).
39. Atomi, H., Fukui, T., Kanai, T., Morikawa, M. & Imanaka, T. Description of *Thermococcus kodakaraensis* sp. nov., a well studied hyperthermophilic archaeon previously reported as *Pyrococcus* sp. KOD1. *Archaea* **1**, 263–267 (2004).
40. Robb, F.T. & Place, A.R. *Archaea: a Laboratory Manual* (Cold Spring Harbor Laboratory Press, Cold Spring Harbor, NY, 1995).
41. Kanai, T. *et al.* A global transcriptional regulator in *Thermococcus kodakaraensis* controls the expression levels of both glycolytic and gluconeogenic enzyme–encoding genes. *J. Biol. Chem.* **282**, 33659–33670 (2007).
42. Kanai, T., Takedomi, S., Fujiwara, S., Atomi, H. & Imanaka, T. Identification of the Phr-dependent heat shock regulon in the hyperthermophilic archaeon, *Thermococcus kodakaraensis*. *J. Biochem.* **147**, 361–370 (2010).
43. Sato, T. *et al.* Genetic evidence identifying the true gluconeogenic fructose-1,6-bisphosphatase in *Thermococcus kodakaraensis* and other hyperthermophiles. *J. Bacteriol.* **186**, 5799–5807 (2004).